Three-dimensional hollow fiber type of carbon nanotube electrode for enhanced ion adsorption capacity

Mi-Young Lee[a], Heeyoung Kim[a], Jong-Oh Kim[b], Seoktae Kang[a],*

[a]*Department of Civil and Environmental Engineering, KAIST, Daejeon 34141, Korea, Tel. +82 42 350 3635; Fax: +82 42 350 3610; emails: stkang@kaist.ac.kr (S. Kang), mylee89@kaist.ac.kr (M.-Y. Lee), hy449@kaist.ac.kr (H. Kim)*
[b]*Department of Civil and Environmental Engineering, Hanyang University, Seoul 04763, Korea, Tel. +82 2 2220 0325; Fax: +82 2 2220 1945; email: jk120@hanyang.ac.kr*

ABSTRACT

In this study, a hollow fiber type of carbon nanotube (HF-CNT) network was fabricated as an electrode material for the improved ion removal in capacitive deionization (CDI). The Raman spectrum proved that the HF-CNT electrode synthesized by wet spinning and subsequent calcination techniques was composed of a porous CNT network. The Brunauer–Emmett–Teller surface area of the HF-CNT was 55.6 m^2/g, and specific capacitance was 23.8 F/g with excellent electrical stability in repeated current–voltage cycling. Accordingly, the HF-CNT electrode showed considerable electrosorption capacity of 58.2 mg/g (18.9 mg/cm^3) in an NaCl concentration of 500 mg/L at 1.2 V. The excellent electrochemical properties of the HF-CNT could be attributed to reduced resistance for ion transport and adsorption by its unique structure. In this study, the three-dimensional HF-CNT was confirmed as a new type of electrode in CDI, with excellent durability and high ion adsorption capacity.

Keywords: Carbon nanotubes; Three-dimensional electrode; Hollow fiber type of carbon nanotube network; Capacitive deionization

1. Introduction

Desalination technology has been used as a key strategy for drinking water production to cope with the global water shortage [1]. However, most commercialized technologies, including reverse osmosis, involve intensive energy consumption. Thus, cost- and energy-effective processes such as membrane distillation, capacitive deionization (CDI), and electrodialysis have been considered as future desalination technologies [1,2]. Of them, CDI is regarded as an alternative desalination technology, especially for low salt (<500 mg/L) solutions [2]. CDI comprises of two electrodes, and is operated by ion adsorption and desorption in the electrical double layer formed by applying voltage to electrodes. When salted water is introduced, ions in the salt water are electrically adsorbed on the electrode due to the applied voltage, and desalted water can be produced.

Since the performance of CDI is governed by electrode materials, there have been intensive studies regarding new electrode materials with preferred pore-size distribution and high electrical capacitance [2–5]. Carbon-based materials including activated carbon (AC) [5,6], mesoporous carbon [7,8], graphene [9,10], carbon nanotubes (CNTs) [3,7,11], and composite electrodes [12] have been utilized as electrodes because of their electrical conductivity, high surface area, and porosity [2]. However, conventional materials such as AC have struggled with their inherently low electrical capacitance, relatively high ion transfer resistances, and poor durability [3,10]. In particular, limited electrosorption capacity has been reported owing to the electric double layer overlapping effect by the high portion of micropores in their pore structure [5,13]. CNTs can be a potential option for CDI electrodes since it intrinsically has superior electrical capacitance, with excellent mechanical and chemical stability [11]. Moreover, CNT electrodes, which comprise of mesopores

* Corresponding author.

and macropores due to their interconnected structures, are beneficial for ion transport [3,14].

However, a major problem of CNTs as CDI electrodes is its intensive energy and binding material consumption during the preparation of CNTs as flat sheet types [3,4,11,15,16]. Current applications of CNT electrodes are limited to being doped or mixed with supporting materials. In addition, the hydrophobic nature of CNTs hinders the transport and adsorption of ions in salty water, thus the hydrophilic modification of the CNT structure is crucial for the novel application of CNTs as CDI electrode material [17]. Treatment with strong acid is widely used to reduce hydrophobicity of CNTs for enhanced electrosorption capacity [7,14]. In addition, hydrophilic functional groups such as sulfonic and amine groups can also be grafted on the surface of pretreated CNTs for improved surface wettability [17]. However, all of these efforts require additional processes, making the preparation of CNTs complex.

Wei et al. [18] successfully developed freestanding hollow fiber type of CNTs (HF-CNTs) which is electrically conductive using a wet spinning technique. Wet spinning technology is a modified fabrication method of electrospinning, in which CNT solution is squeezed in the water through a spinneret without electrical assistance to synthesize fiber structure. After removing the binding polymers, the HF-CNT maintained the excellent electrical properties of CNTs, and exhibited good wettability of water with structural advantages of the three-dimensional hollow fiber over the two-dimensional flat sheet types. Here, this HF-CNT was applied as electrode material of CDI. Good electrical properties and considerable electrosorption capacity of the HF-CNT electrode were achieved by its structural advantages.

2. Experimental setup

2.1. Materials

Pristine multi-walled carbon nanotubes (MWCNTs) were obtained from Cheap Tubes Inc., USA (diameter 50 nm, length 10–20 μm, COOH functionalized). The *N,N*-dimethylformamide (DMF) and polyvinyl butyral (PVB) resin (Butvar® B-74) were purchased from Sigma-Aldrich and Eastman (USA), respectively.

2.2. Preparation of CDI electrodes

The HF-CNT electrode was prepared according to the wet spinning method reported in previous work [18]. In brief, MWCNTs was mixed with DMF, then PVB was added to the solution (CNTs:DMF:PVB = 1.0:1.3:0.5, in weight). The solution was stirred for 24 h, and wet spinning was performed with deionized (DI) water as bore solution and external coagulation bath. The thermal treatment for a prepared hollow fiber of CNT–PVB composite was then conducted at 350°C for 1 h under Ar atmosphere to remove PVB in the hollow fiber tubes.

2.3. Characterization of HF-CNT

The cross-sectional morphology of the prepared HF-CNT electrode was examined by field-emission scanning electron microscopy (FE-SEM; SU5000, Hitachi, Japan). The specific surface area (SSA) was measured by the Brunauer–Emmett–Teller (BET) method with N_2 gas adsorption–desorption

isotherms (ASAP2020, Micromeritics, USA). The pore size and distribution of the HF-CNT electrode was determined using the Barrett–Joyner–Halenda (BJH) model from the adsorption isotherm. The crystallinity of the HF-CNT was characterized by high resolution Raman spectrum (LabRAM HR Evolution Visible_NIR, HORIBA, Japan), with excitation light of an He–Ne laser (514 nm). The surface wettability of the HF-CNT before and after calcination was studied by a contact angle analyzer (Phoenix 300 Plus, SEO, Korea). A drop of solvent was placed on the electrode surface, and three different solvents (DI water, ethylene glycol, and hexadecane) were used to calculate the surface energy (γ_s) of the electrodes by using the extended Young–Dupré equation [19]:

$$\left(1 + \cos\theta\right)\gamma_L^{\text{Total}} = 2\left(\sqrt{\gamma_s^{\text{LW}}\gamma_L^{\text{LW}}} + \sqrt{\gamma_s^+\gamma_L^-} + \sqrt{\gamma_s^-\gamma_L^+}\right) \tag{1}$$

where θ is the contact angle, γ is the surface tension, subscripts s and L indicate solid surface and liquid drop, and superscripts + and – are electron-acceptor and electron-donor contributions to the surface tension, and LW and AB refer to Lifshitz–van der Waals interactions and Lewis acid–base interactions, respectively.

2.4. Electrochemical characterization

Cyclic voltammetry (CV) of the HF-CNT electrode was measured using an electrochemical workstation (VSP-300, Bio-Logic Science Instruments, France) with a typical three-electrode system at ambient temperature. The HF-CNT, a graphite rod, and a saturated calomel electrode (SCE, +0.241 V vs. SHE) were used as the working, counter, and reference electrode, respectively. The active length of all electrodes was fixed at 1 cm during the electrochemical test. The electrolyte was 1 M NaCl solution, and the sweep potential range was adjusted from –0.2 to 0.6 V (vs. SCE). The specific capacitance was calculated from the CV curve by integrating the responsive current according to the following equation [10]:

$$C = \frac{\int_{E_1}^{E_2} i(E)dE}{2\left(E_2 - E_1\right) \cdot m \cdot v_{\text{scan}}} \tag{2}$$

where i is the response current (A) at the frequency range, E_1 and E_2 are cut-off potential (V), v is the potential scan rate (mV/s), and m is the mass of the electrodes (g). For volume-based calculation, effective volume (cm^3) of the HF-CNT was used instead of the mass, which is the subtraction of the inner hollow volume from the total volume of the HF-CNT. During the electrochemical impedance analysis measurement, an electrochemical workstation (ZIVE SP1, WonATech, Korea) was utilized, and a frequency ranging from 0.1 Hz to 1 MHz, and an alternating current amplitude of 5 mV was applied.

2.5. Batch-mode CDI operation

The batch-mode experiments were conducted in a custom-made CDI cell, where a stainless steel needle was attached inside of each chamber as a current collector.

The fabricated HF-CNT electrode was used as both anode and cathode electrodes with an effective length of 2.1 cm.

Different concentration of sodium chloride (NaCl) was tested from 25 to 500 mg/L, and the volume in the cell was at 3.1 mL. Accordingly, the correlation of conductivity (μS/cm) and concentration (mg/L) was calibrated prior to experiment. The applied voltage was 1.2 V, and all experiments were conducted at room temperature. The mass and volume specific ion removal capacities were calculated as follows:

$$\text{Ion removal capacity(mg/g or mg/cm}^3) = \frac{(C_0 - C_t) \times V}{m \text{ or } v_{effective}} \quad (3)$$

where C_0 and C_t (mg/L) are the initial and final NaCl concentrations, V is the volume of the solution (L), m is the mass of electrodes (g), and $v_{effective}$ is the effective volume of HF-CNT (cm^3).

3. Results and discussion

3.1. Physicochemical properties of HF-CNT

The HF-CNTs were successfully synthesized by the wet spinning process. From the SEM images (Fig. 1(a)), fabricated HF-CNT showed randomly entangled CNTs structures, and formed porous structures both on the surface and on the inside structure of the fiber, which is beneficial for electrosorption [3]. The diameter of the HF-CNT was around 930 μm consisting of an inner hollow (~580 μm) and wall layer (~243 μm). Raman spectroscopy was analyzed to identify the surface structures and two characteristic peaks of 1,348 and 1,576 cm^{-1} were presented in the HF-CNT (Fig. 1(b)). The former is known as the D-band, associated with the vibrations of carbon atoms in the defect graphite structure, and the latter is the G-band, reflecting the structural intensity of the sp^2-hybridized carbon atoms. The upshift of the G-band for the HF-CNT from 1,563 cm^{-1} for pristine CNTs could be from the COOH-functional groups by pretreatment [20]. The intensity ratio of the D-band to G-band (I_D/I_G) value of the HF-CNT increased from 0.60 to 0.65 after calcination. This increased value of I_D/I_G could represent the enhanced pore density and a greater degree of wall graphitization, suggesting improved structural quality of the HF-CNT by thermal treatment [4,21]. In addition, it could be found that the intensity of a peak associated with the PVB (1,114 cm^{-1} for ester groups) decreased after calcination. Then, spaces could be posed by removal of the PVB, resulting in pores, which are beneficial for the accumulation and transport of charges during adsorption process [4]. Meanwhile, there barely remained intensity in the peak of 1,114 cm^{-1} after calcination. The residual amount of the PVB in the calcined sample was estimated to be 1.8% of the total mass by thermogravimetric analysis, as shown in Fig. 1(c). Since a higher heating temperature tends to result in the hydrophobic property of carbon materials, the HF-CNT was calcined at 350°C, which is enough to remove PVB.

The BET results are shown in Fig. 2, and the surface area and total pore volume of HF-CNT were 55.56 m^2/g and 0.25 cm^3/g, respectively. The pore size of the HF-CNT ranged from 7 to 100 nm, with an average pore size of 43.45 nm by

BJH theorem, indicating the mesopore structures. This could ensure a relatively higher mass-transfer compared with conventional carbon-based electrodes [14], and allow the hydrated salt ions to be easily transported through the pores, leading to advantages for ion adsorption [11].

The contact angle of water droplets on the surface of fabricated HF-CNT is illustrated in Fig. 3. The contact angle with DI water decreased from 103.8° to 45.4°, and calculated surface free energy (γ_s) improved from 27.74 to 45.77 mJ/m^2 after the calcination process, indicating increased surface wettability (Table 1). The enhanced wettability of HF-CNT after thermal treatment could be the consequence of the increased surface roughness and pores as shown in Fig. 1. Park and Choi [22]
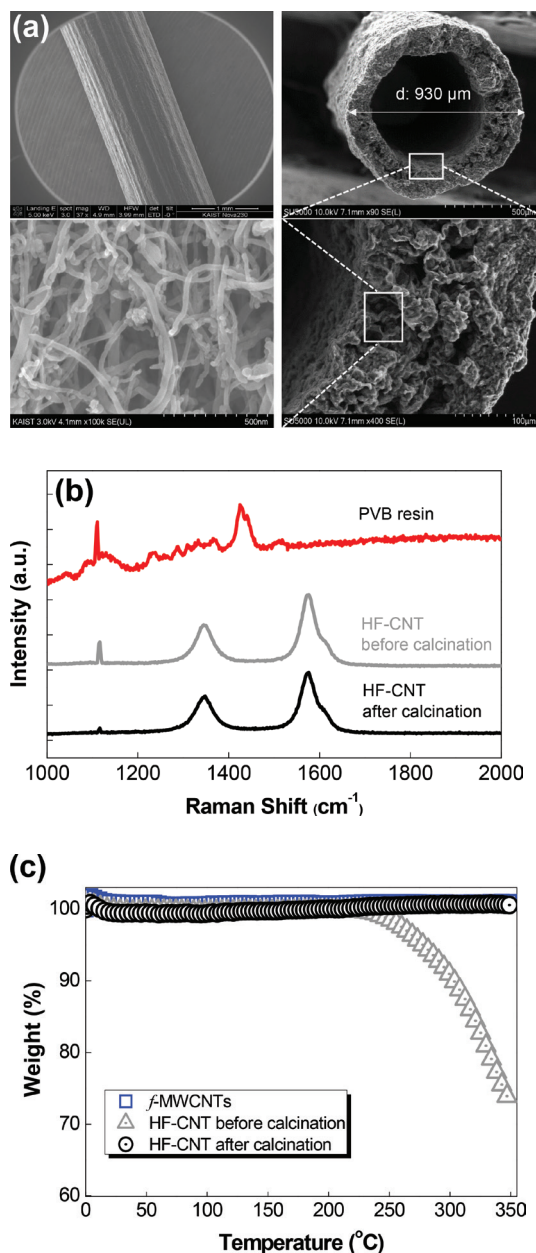
Fig. 1. The physical characterization of the HF-CNT, showing: (a) the SEM images, (b) Raman spectroscopy, and (c) thermogravimetric analysis.
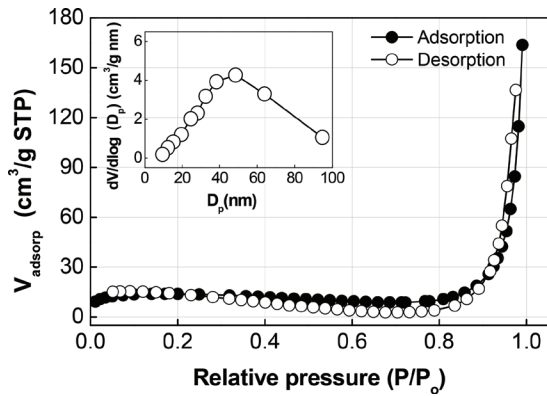
Fig. 2. The N$_2$ adsorption/desorption isotherms – inset is the BJH pore-size distribution.
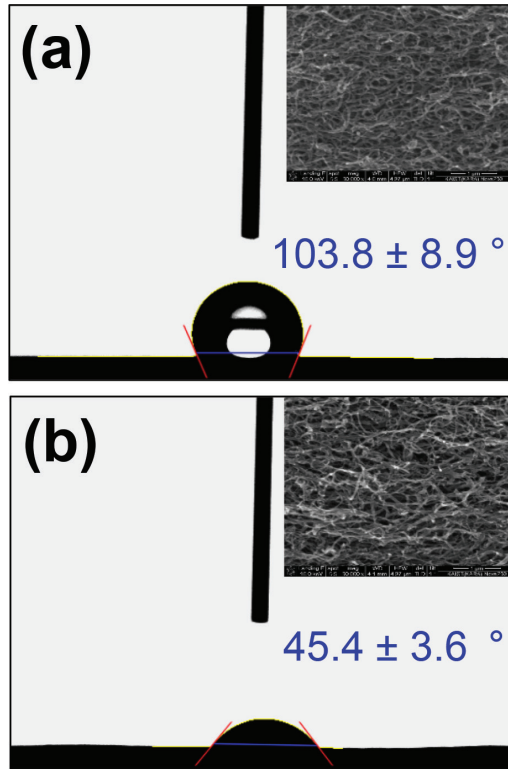
Fig. 3. Surface contact angle analysis for HF-CNT electrodes: (a) before and (b) after calcination.

Table 1
Contact angle with tested liquids and calculated surface free energy of the HF-CNT

Liquid	Contact angle (°)	
	Before calcination	After calcination
Water	103.8 ± 8.9	45.4 ± 3.6
Ethylene glycol	85.5 ± 1.7	15.8 ± 1.8
Hexadecane	15.9 ± 0.8	12.9 ± 0.9
Surface free energy (γ_s, mJ/m^2)	27.7	45.8

demonstrated that the hydrophilic surface is more favorable for ions to access inner adsorption sites. Hence, the decrease of contact angle after thermal treatment could be attributed to the increased ion adsorption capacity during CDI.

3.2. Electrochemical properties of HF-CNT

The electrochemical behavior of the electrode was examined using a CV test. Fig. 4(a) exhibits the cyclic voltammograms of the HF-CNT in 1 M NaCl solution with scan rates of 1, 20, 50, 80, and 100 mV/s. The CV curves represented a rectangular
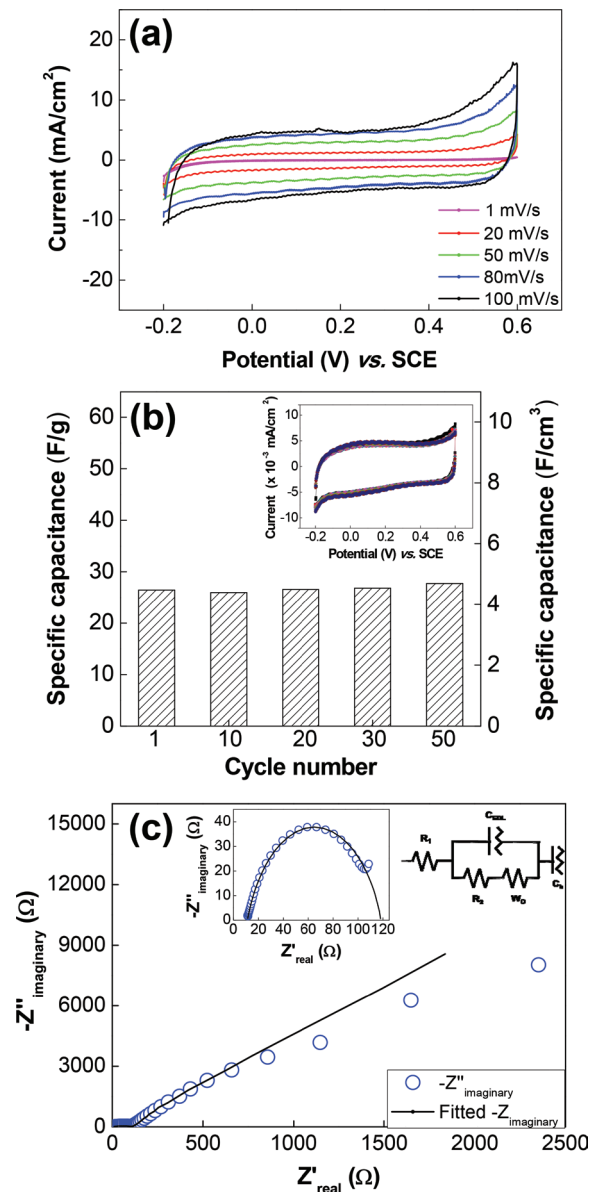
Fig. 4. The electrochemical characterization of HF-CNT electrode showing: (a) CV curves of the HF-CNT in 1 M NaCl solution with scan rates of 1, 20, 50, 80, and 100 mV/s, (b) change of specific capacitance after 50 cycles at scan rate of 50 mV/s, and (c) the Nyquist plot of the CDI cell with 1 M NaCl solution – inset is the Warburg semi-circle and corresponding equivalent circuit.

shape without electrochemical oxidation/reduction peak in the entire potential range, ensuring that ions are adsorbed by electrostatic attraction [10]. The calculated capacitance showed only 27% reduction with increase of potential sweep, indicating stable mass transfer and ion adsorption capacity for the HF-CNT owing to its well-distributed pore structures [10,23]. To identify the stability and regeneration of the HF-CNT, CV profiles were repeated at a high scan rate (50 mV/s) up to 50 times. The result indicated excellent retention of specific capacitance after 50 cycles of potential sweep, showing good cyclic stability (Fig. 4(b)).

The analysis of electrochemical impedance was illustrated as the Nyquist plot, and it was fitted to calculate the resistances by an equivalent circuit, as shown in the inset of Fig. 4(c). The fitting was qualified by chi-squared parameter, which is the sum of the square of the differences between measured and simulated data. The HF-CNT showed one semi-circle at high frequency and a straight line at low frequency in the Nyquist plot. The plot for the low frequency, characteristic of semi-infinite diffusion (called Warburg resistance, W_o), represented typical double layer capacitive behavior with the 45° line angle [24,25]. The ohmic resistance (R_1) of the HF-CNT was relatively small (10.8 Ω) compared with the flat type of CNT electrodes (12–30 Ω) [7]. The arc corresponds to the resistances at the interfaces of the current collector/active material as well as of the electrode/electrolyte

(known as polarization resistance). The polarization resistance (R_2) for the HF-CNT, calculated by the diameter of the semi-circle, was relatively high (89.4 Ω). Previous studies demonstrated that for carbon-based electrodes, poor contact with a metal-based current collector resulted in the increase of polarization resistance [26–28]. The relatively high polarization resistance for the HF-CNT could be attributed to the decrease of electrical conductivity between the stainless steel and the HF-CNT. Consequently, various current collectors should be tested for the minimization of polarization resistance in the future research.

3.3. Ion adsorption capacity

Fig. 5 shows the electrosorption capacity for the fabricated HF-CNT electrode. The initial conductivity for 100 mg/L of NaCl dropped rapidly, which decelerated after 5 min and reached a saturated value in 30 min as shown in Fig. 5(a). The repeated ion adsorption capacity of the HF-CNT showed stable performance during 10 cycles indicating good reproducibility (Figs. 5(b) and (c)). Fig. 5(d) shows the ion adsorption capacity of the HF-CNT at different salt concentrations from 25 to 500 mg/L. The HF-CNT exhibited gradual improvement of ion removal capacities from 3.8 to 58.2 mg/g, for 25 and 500 mg/L, respectively. From our knowledge, this value is the highest electrosorption capacity for carbon-based electrodes
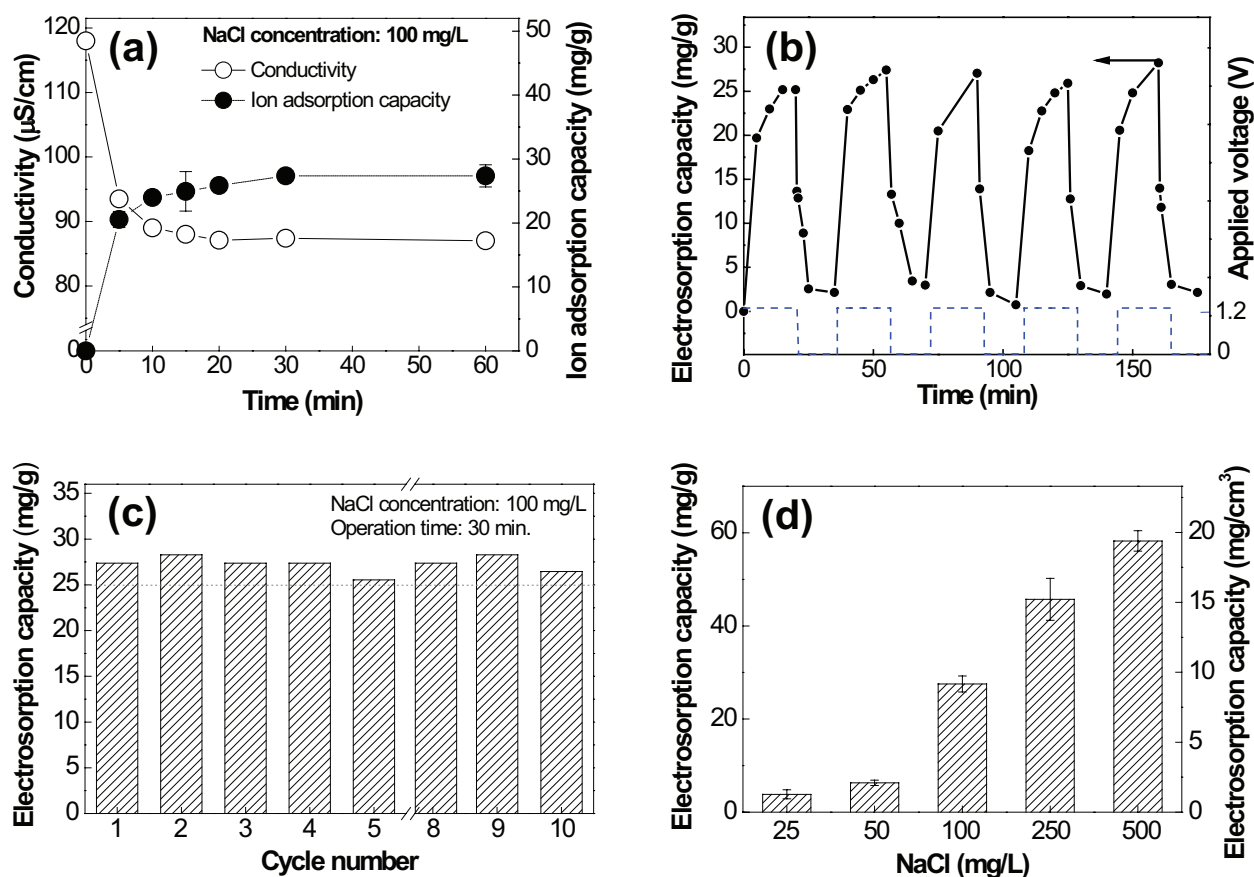
Fig. 5. CDI performance showing: (a) change of conductivity and electrosorption capacity with time, (b) transient of electrosorption capacity during charging–discharging cycles, (c) stability of electrosorption capacity with 10 cycles, and (d) electrosorption capacities in different salt concentrations.

including single carbon materials, composites, and hybrid electrodes with applied voltage of 1.2 V [3–5,9,11,29–32]. It could be due to both well-distributed pore structures and excellent electrochemical properties of the HF-CNT, resulting in reduced total resistance for ion adsorption [29]. Compared with the references, the HF-CNT showed excellent desalination performance even though its SSA was relatively low (Fig. 6). It has been demonstrated that high SSA alone does not guarantee ion adsorption capacity, since SSA is mainly determined by the portion of micropores through which ions struggles to infiltrate for adsorption [3]. The SSA and salt removal capacity of different electrodes are summarized in Table 2.

The high ion removal capacity with good cyclic stability of the HF-CNT can be related with its unique hollow fiber structure. Unlike synthetic methods for CNTs electrode as flat types, HF-CNT is not influenced by pressurization, which could lead to structural deformation and aggregation of CNTs [9]. In addition, the decrease of electrical conductivity and increase of resistance, which result from the presence of supporting materials (e.g., polymer binders) can be eliminated for the HF-CNT after calcination [26,31]. Accordingly, ion accessibility, diffusion, and adsorption through pores are facilitated with reduced resistance [32]. Even a limited comparison can verify outstanding ion removal capacity for the HF-CNT electrode.

4. Conclusion

Poor synthetic methodology for CNT electrodes offers limited desalination performance as expected. In this paper, an HF-CNT electrode was fabricated and applied to the CDI process for the first time. It was identified by the Raman analysis that there was no structural degradation of the HF-CNT synthesized by the wet spinning method as compared with pristine CNTs. In addition, the HF-CNT indicated well-distributed pore structures from macropores to micropores, and showed good surface wettability. The specific
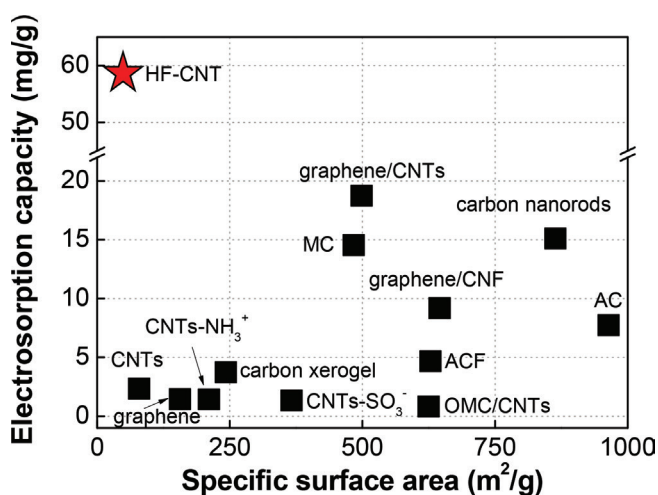
Fig. 6. Comparison of electrosorption capacity for carbon-based electrodes along with the specific surface area at 1.2 V (schematized data from Table 2).

Table 2
Comparison of electrosorption capacity for different electrodes with applied voltage of 1.2 V

Electrode	SSA (m²/g)	Initial NaCl concentration		Electrosorption capacity (mg/g)	Reference
		(µS/cm)	(mg/L)		
HF-CNT	55.6	–	250	45.7	This study
			500	58.2	
CNTs sponge	60–80	–	60	4.3	[11]
CNTs by EPD method	82	100	–	2.3	[4]
Pristine CNTs	444.2	50	–	0.9	[17]
CNTs-SO₃⁻ functionalized	370.8			1.4	
CNTs-NH₃⁺ functionalized	207.8			1.4	
CNTs/OMC	621	–	40	0.7	[7]
Graphene/CNTs sponge	498.2	–	500	18.7	[31]
Graphene	154.7	100	–	1.0	[9]
N-doped graphene	358.9			1.3	
Carbon nanofiber/graphene	649		100	9.2	[10]
Activated carbon fiber	630			4.7	
Mesoporous carbon	488		4,460	14.5	[8]
Activated carbon	964		234	7.6	[5]
Carbon xerogel	239.1	–	260	3.3	[32]
Carbon nanorods	864.1	–	500	15.1	[30]

EPD, electrophoretic deposition; OMC, ordered mesoporous carbon.

capacitance of the HF-CNT electrode was 28.3 F/g, with excellent cyclic stability during 50 cycles. Accordingly, good reproducibility of performance was achieved, and ion adsorption capacity for the HF-CNT was 58.2 mg/g with 500 mg/L NaCl at 1.2 V. This outstanding performance of the HF-CNT electrode was obtained by its unique structure with uniform distribution of pores, which facilitated transport and adsorption of ions. Thus, the high potential of three-dimensional HF-CNT as a new type of electrode was confirmed for enhanced CDI performance.

Acknowledgments

References

[1] M. Elimelech, W.A. Phillip, The future of seawater desalination: energy, technology, and the environment, Science, 333 (2011) 712–717.

[2] M.E. Suss, S. Porada, X. Sun, P.M. Biesheuvel, J. Yoon, V. Presser, Water desalination via capacitive deionization: what is it and what can we expect from it?, Energy Environ. Sci., 8 (2015) 2296–2319.

[3] X.Z. Wang, M.G. Li, Y.W. Chen, R.M. Cheng, S.M. Huang, L.K. Pan, Z. Sun, Electrosorption of ions from aqueous solutions with carbon nanotubes and nanofibers composite film electrodes, Appl. Phys. Lett., 89 (2006) 053127.

[4] C. Nie, L. Pan, H. Li, T. Chen, T. Lu, Z. Sun, Electrophoretic deposition of carbon nanotubes film electrodes for capacitive deionization, J. Electroanal. Chem., 666 (2012) 85–88.

[5] C.H. Hou, C.Y. Huang, A comparative study of electrosorption selectivity of ions by activated carbon electrodes in capacitive deionization, Desalination, 314 (2013) 124–129.

[6] B. Jia, W. Zhang, Preparation and application of electrodes in capacitive deionization (CDI): a state-of-art review, Nanoscale Res. Lett., 11 (2016) 1–25.

[7] Z. Peng, D. Zhang, T. Yan, J. Zhang, L. Shi, Three-dimensional micro/mesoporous carbon composites with carbon nanotube networks for capacitive deionization, Appl. Surf. Sci., 282 (2013) 965–973.

[8] C. Tsouris, R. Mayes, J. Kiggans, K. Sharma, S. Yiacoumi, D. DePaoli, S. Dai, Mesoporous carbon for capacitive deionization of saline water, Environ. Sci. Technol., 45 (2011) 10243–10249.

[9] X. Xu, L. Pan, Y. Liu, T. Lu, Z. Sun, Enhanced capacitive deionization performance of graphene by nitrogen doping, J. Colloid Interface Sci., 445 (2015) 143–150.

[10] G. Wang, Q. Dong, T. Wu, D. Zhan, M. Zhou, J. Qiu, Ultrasound-assisted preparation of electrospun carbon fiber/graphene electrodes for capacitive deionization: importance and unique role of electrical conductivity, Carbon, 103 (2016) 311–317.

[11] L. Wang, M. Wang, Z.H. Huang, T. Cui, X. Gui, F. Kang, K. Wang, D. Wu, Capacitive deionization of NaCl solutions using carbon nanotube sponge electrodes, J. Mater. Chem., 21 (2011) 18295–18299.

[12] A.S. Yasin, H.O. Mohamed, I.M.A. Mohamed, H.M. Mousa, N.A.M. Barakat, Enhanced desalination performance of capacitive deionization using zirconium oxide nanoparticles-doped graphene oxide as a novel and effective electrode, Sep. Purif. Technol., 171 (2016) 34–43.

[13] K.L. Yang, S. Yiacoumi, C. Tsouris, Electrosorption capacitance of nanostructured carbon aerogel obtained by cyclic voltammetry, J. Electroanal. Chem., 540 (2003) 159–167.

[14] S. Chung, H. Kang, J.D. Ocon, J.K. Lee, J. Lee, Enhanced electrical and mass transfer characteristics of acid-treated carbon nanotubes for capacitive deionization, Curr. Appl. Phys., 15 (2015) 1539–1544.

[15] H. Li, S. Liang, M. Gao, G. Li, J. Li, L. He, The study of capacitive deionization behavior of a carbon nanotube electrode from the perspective of charge efficiency, Water Sci. Technol., 71 (2015) 83–88.

[16] Y. Liu, J. Ma, T. Lu, L. Pan, Electrospun carbon nanofibers reinforced 3D porous carbon polyhedra network derived from metal-organic frameworks for capacitive deionization, Sci. Rep., 6 (2016) 32784.

[17] J. Yang, L. Zou, N.R. Choudhury, Ion-selective carbon nanotube electrodes in capacitive deionisation, Electrochim. Acta, 91 (2013) 11–19.

[18] G. Wei, S. Chen, X. Fan, X. Quan, H. Yu, Carbon nanotube hollow fiber membranes: high-throughput fabrication, structural control and electrochemically improved selectivity, J. Membr. Sci., 493 (2015) 97–105.

[19] B. He, N.A. Patankar, J. Lee, Multiple equilibrium droplet shapes and design criterion for rough hydrophobic surfaces, Langmuir, 19 (2003) 4999–5003.

[20] Y.S. Li, J.L. Liao, S.Y. Wang, W.H. Chiang, Intercalation-assisted longitudinal unzipping of carbon nanotubes for green and scalable synthesis of graphene nanoribbons, Sci. Rep., 6 (2016) 22755.

[21] S. Song, S. Jiang, Selective catalytic oxidation of ammonia to nitrogen over CuO/CNTs: the promoting effect of the defects of CNTs on the catalytic activity and selectivity, Appl. Catal., B, 117–118 (2012) 346–350.

[22] B.H. Park, J.H. Choi, Improvement in the capacitance of a carbon electrode prepared using water-soluble polymer binder for a capacitive deionization application, Electrochim. Acta, 55 (2010) 2888–2893.

[23] X. Du, P. Guo, H. Song, X. Chen, Graphene nanosheets as electrode material for electric double-layer capacitors, Electrochim. Acta, 55 (2010) 4812–4819.

[24] S.C. Yang, J. Choi, J. Yeo, S. Jeon, H. Park, D.K. Kim, Flow-electrode capacitive deionization using an aqueous electrolyte with a high salt concentration, Environ. Sci. Technol., 50 (2016) 5892–5899.

[25] N.-L. Liu, S. Dutta, R.R. Salunkhe, T. Ahamad, S.M. Alshehri, Y. Yamauchi, C.-H. Hou, K.C.-W. Wu, ZIF-8 derived, nitrogen-doped porous electrodes of carbon polyhedron particles for high-performance electrosorption of salt ions, Sci. Rep., 6 (2016) 28847.

[26] Y. Qu, T.F. Baumann, J.G. Santiago, M. Stadermann, Characterization of resistances of a capacitive deionization system, Environ. Sci. Technol., 49 (2015) 9699–9706.

[27] C. Lei, F. Markoulidis, Z. Ashitaka, C. Lekakou, Reduction of porous carbon/Al contact resistance for an electric double-layer capacitor (EDLC), Electrochim. Acta, 92 (2013) 183–187.

[28] H.-C. Wu, Y.-P. Lin, E. Lee, W.-T. Lin, J.-K. Hu, H.-C. Chen, N.-L. Wu, High-performance carbon-based supercapacitors using Al current-collector with conformal carbon coating, Mater. Chem. Phys., 117 (2009) 294–300.

[29] F. Xing, T. Li, J. Li, H. Zhu, N. Wang, X. Cao, Chemically exfoliated MoS₂ for capacitive deionization of saline water, Nano Energy, 31 (2017) 590–595.

[30] Y. Liu, L. Pan, X. Xu, T. Lu, Z. Sun, D.H.C. Chua, Carbon nanorods derived from natural based nanocrystalline cellulose for highly efficient capacitive deionization, J. Mater. Chem. A, 2 (2014) 20966–20972.

[31] X. Xu, Y. Liu, T. Lu, Z. Sun, D.H.C. Chua, L. Pan, Rational design and fabrication of graphene/carbon nanotubes hybrid sponge for high-performance capacitive deionization, J. Mater. Chem. A, 3 (2015) 13418–13425.

[32] J. Landon, X. Gao, B. Kulengowski, J.K. Neathery, K. Liu, Impact of pore size characteristics on the electrosorption capacity of carbon xerogel electrodes for capacitive deionization, J. Electrochem. Soc., 159 (2012) A1861–A1866.

Supporting materials
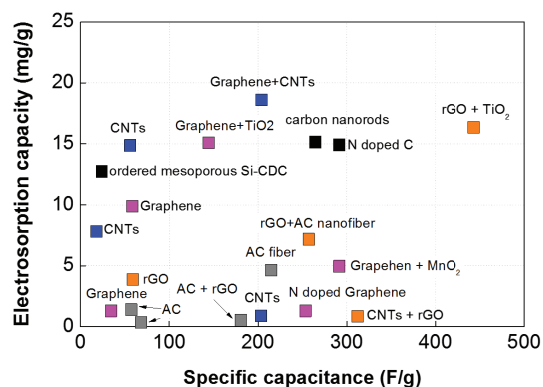
Fig. S1. Comparison of ion adsorption capacity with specific capacitance for carbon-based electrode.

Table S1
Specific capacitance and electrosorption capacity for carbon based electrode

Electrode materials	Specific capacitance (F/g)	Electrosorption capacity (EC, mg/g)	Reference
Activated carbon (AC)	54.6	1.2	[1]
Graphene	58.5	9.9	
Graphene + TiO$_2$ 16 wt%	142.6	15.1	
AC	67	0.2	[2]
AC + rGO 20 wt%	181	0.55	
AC fiber	214	4.7	[3]
rGO 10% + AC fiber	256	7.2	
Graphene	206.01	0.96	[4]
N-doped graphene	253.06	1.29	
Graphene + MnO$_2$	292	5.01	[5]
Graphene + CNTs sponge	203.48	18.7	[6]
Graphene	35.2	1.27	[7]
3D-grphene	58.4	1.97	
CNTs	202	0.87	[8]
CNTs + rGO 10 wt%	311.1	0.88	
rGO	59	3.94	[9]
rGO + TiO$_2$ 20 wt%	443	16.4	
Carbon nanorods	264.2	15.12	[10]
CNTs	17.8	7.86	[11]
Acid treated CNTs	55.8	14.82	
Carbon xerogel	28.6	3.3	[12]
N-doped carbon sphere	290.74	14.91	[13]
Ordered mesoporous Si-CDC	22.3	12.8	[14]

rGO, reduced graphene oxide; CDC, carbide derived carbon.

References

[1] H. Yin, S. Zhao, J. Wan, H. Tang, L. Chang, L. He, H. Zhao, Y. Gao, Z. Tang, Three-dimensional graphene/metal oxide nanoparticle hybrids for high-performance capacitive deionization of saline water, Adv. Mater., 25 (2013) 6270–6276.

[2] H. Li, L. Pan, C. Nie, Y. Liu, Z. Sun, Reduced graphene oxide and activated carbon composites for capacitive deionization, J. Mater. Chem., 22 (2012) 15556–15561.

[3] Q. Dong, G. Wang, B. Qian, C. Hu, Y. Wang, J. Qiu, Electrospun composites made of reduced graphene oxide and activated carbon nanofibers for capacitive deionization, Electrochim. Acta, 137 (2014) 388–394.

[4] X. Xu, L. Pan, Y. Liu, T. Lu, Z. Sun, Enhanced capacitive deionization performance of graphene by nitrogen doping, J. Colloid Interface Sci., 445 (2015) 143–150.

[5] A.G. El-Deen, N.A.M. Barakat, H.Y. Kim, Graphene wrapped MnO$_2$-nanostructures as effective and stable electrode materials for capacitive deionization desalination technology, Desalination, 344 (2014) 289–298.

[6] X. Xu, Y. Liu, T. Lu, Z. Sun, D.H.C. Chua, L. Pan, Rational design and fabrication of graphene/carbon nanotubes hybrid sponge for high-performance capacitive deionization, J. Mater. Chem. A, 3 (2015) 13418–13425.

[7] H. Wang, D. Zhang, T. Yan, X. Wen, J. Zhang, L. Shi, Q. Zhong, Three-dimensional macroporous graphene architectures as high performance electrodes for capacitive deionization, J. Mater. Chem. A, 1 (2013) 11778–11789.

[8] H. Li, S. Liang, J. Li, L. He, The capacitive deionization behaviour of a carbon nanotube and reduced graphene oxide composite, J. Mater. Chem. A, 1 (2013) 6335–6341.

[9] A.G. El-Deen, J.-H. Choi, C.S. Kim, K.A. Khalil, A.A. Almajid, N.A.M. Barakat, TiO$_2$ nanorod-intercalated reduced graphene oxide as high performance electrode material for membrane capacitive deionization, Desalination, 361 (2015) 53–64.

[10] Y. Liu, L. Pan, X. Xu, T. Lu, Z. Sun, D.H.C. Chua, Carbon nanorods derived from natural based nanocrystalline cellulose for highly efficient capacitive deionization, J. Mater. Chem. A, 2 (2014) 20966–20972.

[11] S. Chung, H. Kang, J.D. Ocon, J.K. Lee, J. Lee, Enhanced electrical and mass transfer characteristics of acid-treated carbon nanotubes for capacitive deionization, Curr. Appl. Phys., 15 (2015) 1539–1544.

[12] J. Landon, X. Gao, B. Kulengowski, J.K. Neathery, K. Liu, Impact of pore size characteristics on the electrosorption capacity of carbon xerogel electrodes for capacitive deionization, J. Electrochem. Soc., 159 (2012) A1861–A1866.

[13] Y. Liu, T. Chen, T. Lu, Z. Sun, D.H.C. Chua, L. Pan, Nitrogen-doped porous carbon spheres for highly efficient capacitive deionization, Electrochim. Acta, 158 (2015) 403–409.

[14] S. Porada, L. Borchardt, M. Oschatz, M. Bryjak, J.S. Atchison, K.J. Keesman, S. Kaskel, P.M. Biesheuvel, V. Presser, Direct prediction of the desalination performance of porous carbon electrodes for capacitive deionization, Energy Environ. Sci., 6 (2013) 3700–3712.